HEFAT2014
10th International Conference on Heat Transfer, Fluid Mechanics and Thermodynamics
14 – 16 July 2014
Orlando, Florida

COMPUTATIONAL FLUID DYNAMICS SIMULATION AND TURBOMACHINERY CODE VALIDATION OF A HIGH PRESSURE RATIO RADIAL-INFLOW TURBINE

M. Odabaee[a], E. Sauret[b], K. Hooman[a]
[a] School of Mechanical and Mining Engineering, The University of Queensland, St Lucia, Brisbane, QLD, 4072, Australia
[b] Science and Engineering Faculty, Queensland University of Technology, Brisbane, QLD, 4000, Australia

E-mail: m.odabaee@uq.edu.au

ABSTRACT

The present study explores reproducing the closest geometry of a high pressure ratio single stage radial-inflow turbine applied in the Sundstrans Power Systems T-100 Multipurpose Small Power Unit. The commercial software ANSYS-Vista RTD along with a built in module, BladeGen, is used to conduct a meanline design and create 3D geometry of one flow passage. Carefully examining the proposed design against the geometrical and experimental data, ANSYS-TurboGrid is applied to generate computational mesh. CFD simulations are performed with ANSYS-CFX in which three-dimensional Reynolds-Averaged Navier-Stokes equations are solved subject to appropriate boundary conditions. Results are compared with numerical and experimental data published in the literature in order to generate the exact geometry of the existing turbine and validate the numerical results against the experimental ones.

INTRODUCTION

The radial-inflow turbine is a rugged turbine, designed to run under severe gas conditions and applied in internal combustion engines, natural gas, diesel, and gasoline power units. Since the radial-inflow turbine has a higher tip speed than an axial turbine, the amount of work produced by a single stage would be equal to that of two or more stages in an axial turbine [1].

In order to predict turbine characteristics, it is essential to compute flow field throughout the turbine, analyse the flow passage where viscous three dimensional rotational/curvature and turbulence effects play significant roles. Although there are few experimental published studies on radial turbines providing enough information in the literature [2-5], there is an ongoing demand of well-documented configurations of radial-inflow turbines in order to develop reliable numerical simulations, validated by experimental investigations. CFD simulations have been conducted to achieve a better understanding of the flow characteristics, including grid refinements and independency, and the validation of numerical results (1D & 3D) as discussed in [6-12]. Considering the numerical simulations on radial-inflow turbines available in the literature, the necessary geometric pieces of information are not available in published documents. Therefore, one cannot reproduce the complete configuration in order to conduct CFD simulations, followed by comparisons against the performed experiments [13].

However, Sauret [13] provided a fully open set of data and recreated the exact geometry of the high pressure ratio single stage radial-inflow turbine used in [5]. The study includes a preliminary 1D design using RITAL and checked against Hamilton Sundstrand and available experimental data [5]. The 3D geometry was created by Axcent and fully detailed in terms of rotor and stator blade profiles, thicknesses and angles. Axcent-PushButton CFD has been applied as the solver to perform the 3D viscous flow simulations where the effect of the tip clearance gap was investigated in detail for a range of operating conditions.

Following the geometrical data provided in [13], the present study recreates the 3D geometry of the identical turbine applying commercially available CFD software ANSYS turbomachinery package in which the Vista RTD is used to conduct a meanline design and BladeGen is applied to create 3D geometry of rotor and stator blades. A numerical study is performed by ANSYS-CFX for two operating conditions and results are compared with numerical and experimental data (1D and 3D analyses) presented in [13]. The main purpose of the abovementioned process is conducting a CFD simulation and code validation study of a radial-inflow turbine started by Sauret [13] to further investigate a new supercritical radial-

inflow turbine developed by Queensland Geothermal Energy Centre of Excellence.

NOMENCLATURE

C_P	[-]	Pressure recovery coefficient
P	[kPa]	Pressure
T	[K]	Temperature
U	[m/s]	Absolute velocity
y^+	[-]	Grid spacing

Special characters

η	[%]	Efficiency
β	[deg]	Blade angle
ω	[RPM]	Rotational speed

Subscripts

d	Diffuser
in	Inlet
out	Outlet
r	Rotor
s	Stator
S	Static
T	Total
T-S	Total-to-Static
T-T	Total-to-Total

MEANLINE ANALYSIS

The preliminary design procedure addresses the basic stage components defining the inlet volute, nozzle row, rotor and exhaust diffuser, providing an aerodynamic design that completely achieves a design with required outputs. There are several meanline methodologies based on the analysis of the flow along mean streamline through the stage components [14].

In this study, the meanline design of the radial turbine is conducted by ANSYS-Vista RTD developed by PCA Engineers and integrated in ANSYS BladeModeler software. To re-calculate the overall performances of the turbine the aerodynamic and geometry data provided in [13] are used as input to Vista RTD. The required aerodynamics inputs are inlet stagnation temperature and pressure, mass flow rate, total-to-total expansion ratio, rotational speed and blade speed ratio [13], stage and nozzle efficiencies, fluid properties and inlet and exit flow angles. For geometrical inputs, the number of vanes, impeller diameters and axial length are given.

3D GEOMETRY

To define the 3D geometry of the turbine, initial geometrical data from preliminary design (Vista RTD) were exported to ANSYS-BladeGen in which the 3D nozzle and rotor blades were created. The geometrical data from [13] including nozzle hub and shroud thicknesses (similar on hub and shroud), nozzle blade profile (adjusted by Piecewise linear curves), rotor hub and shroud contours and rotor blade angle and thickness distributions for both hub and shroud separately (adjusted by Piecewise linear curve) were applied in order to define an identical turbine. Figure 1 shows the thickness distribution of rotor blade from hub (Span 0) to shroud (Span 1) along the meridional axis from leading edge to trailing edge, where three additional layers (Span 0.25, 0.5 and 0.75) are placed at different heights of blade. Rotor blade angle (β) distribution from hub to shroud is also plotted in Figure 2.

Stator blade angle and thickness distributions are demonstrated in Figure 3 and 4 respectively where the thickness and blade values from hub to shroud are identical. One should notice that BladeGen cannot create the exact pure conical shape of the diffuser; similar issue was reported in [13] with Axcent. To overcome this problem, the 3D diffuser geometry was generated using ANSYS-Geometry separately, considering the correct dimensions of the diffuser.

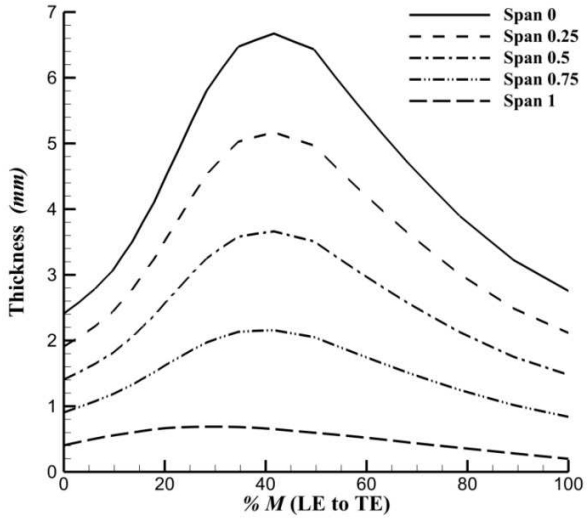

Figure 1 Rotor blade thickness distribution from hub (Span 0) to shroud (Span 1) vs. meridional axis (from leading to trailing edge)

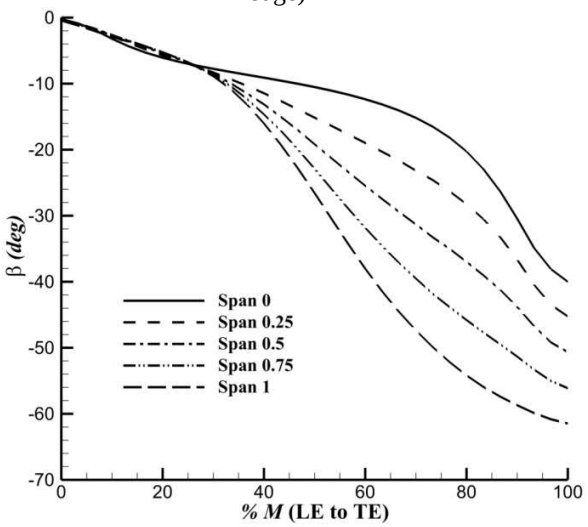

Figure 2 Rotor blade angle distribution from hub (Span 0) to shroud (Span 1) vs. meridional axis (from leading to trailing edge)

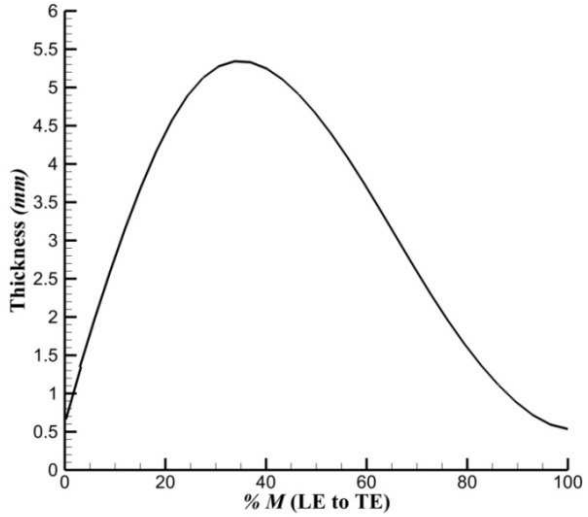

Figure 3 Stator blade thickness distribution from hub (Span 0) to shroud (Span 1) vs. meridional axis (from leading to trailing edge)

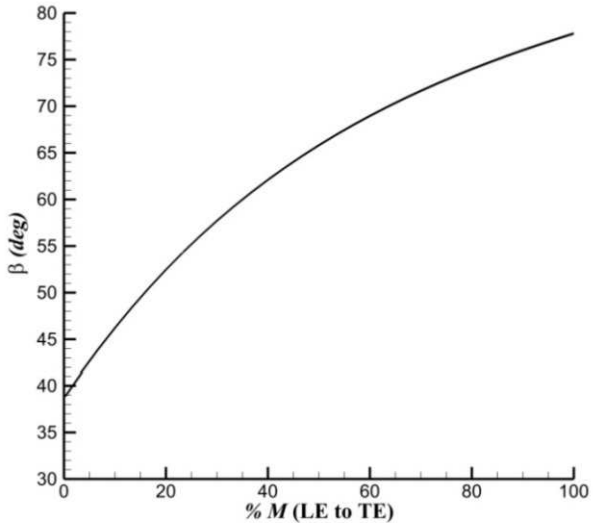

Figure 4 Stator blade angle distribution from hub (Span 0) to shroud (Span 1) vs. meridional axis (from leading to trailing edge)

COMPUTATIONAL SIMULATION

There two numerical cases defined to compare present CFD results with results provided in [5, 13]: rig condition (ω = 71700 RPM) with tip clearance and engine (ω = 106588 RPM) condition with tip clearance. For both cases, mesh generation study and CFD solver setup will be disgust in details.

Mesh Generation

ANSYS-TurboGrid was applied to generate the flow passage meshes for both rotor and stator where the Automatic Topology and Meshing (ATM Optimized) option was used in stator and rotor flow passages without the "cut-off squared" option at trailing edges. This generates a high quality mesh avoiding negative volumes whi are problematic for traditional mesh generations [15]. Variable normal distances at leading and trailing edges of rotor were defined in TurboGrid to generate mesh for the shroud tip clearance volume, as mentioned in [5, 13].

For the boundary layer refinement control, the first element method was used and Reynolds number is 4×10^6 with Near Wall Element Size Specification to meet the *y+* requirement for turbulence model, ranged from 6 to 147. The individual diffuser was imported into ANSYS-Mesh and Tetrahedrons Method was used to generate a fine mesh, as shown in Appendix Figure 11. After checking grid refinement and mesh quality, the total grid number is 748484 –including stator, rotor, and diffuser- where the final mesh analysis of rotor and stator flow passages shows 30° for minimum face angle, 155° for maximum face angle with a positive minimum volume. Figures 4 and 5 illustrate the 3D views of rotor and stator blade flow passages, respectively.

Solver and Boundary Conditions

The mesh from ANSYS-TurboGrid was imported into ANSYS CFX to conduct the 3D viscous flow simulations. *K-ω* turbulence model was chosen as recommended by [16, 17]. The basic settings used for the discretisation of the Reynolds-Averaged Navier-Stokes (RANS) equations - for a steady state solution - are Upwind Advection Scheme and First Order Turbulence Numerics.

Simulation of RANS equations significantly reduces the computational efforts as they merely represent the mean flow quantities whiteout a need for the resolution of the turbulent fluctuations and is generally adopted for practical engineering problems [15]. In this study, the first order scheme (Upwind Advection) is used in order to achieve a better convergence. Therefore, applying a second order scheme results in higher accuracy but slower and less tight convergence.

Boundary conditions are set for both engine and rig conditions where the inlet and outlet total pressures and inlet total temperatures differ at a constant pressure ratio of 5.7. Numbers and letters are used to better describe the Figure. As shown in Figure 6, the inlet conditions are defined at the front (1) of the stator blade (S) while the outlet conditions were specified at the exit (4) of the diffuser (D).

Single flow passage for both stator and rotor (R) is simulated and *Rotational Periodicity* is applied. There are two interfaces placed between the outlet of the stator flow passage and the inlet of the rotor flow passage (2) and the outlet of rotor flow passage and the inlet of the diffuser (3) where both are modelled as a Stage Frame Change/Mixing and Automatic Pitch Change. In Figure 6, the vertical line on the right side of the geometry presents the rotational axis and the arrow on the left side shows the rotation direction of the rotor blade.

The inlet total pressure, inlet total temperature and outlet static pressure of rig and engine condition are defined and set in CFX-Pre, as shown in Table 1. The operating pressure and temperature for rig conditions are lower than those of engine conditions where the inlet total pressure and inlet total temperature are $P_{T,s,in}$= 413.6 kPa and $T_{T,s,in}$= 477.6 K respectively (see [5, 13]).

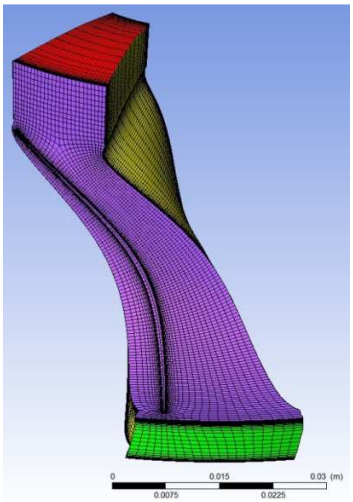

Figure 4 3D view of mesh generated for rotor blade flow passage presenting inlet (green), outlet (red), shroud (purple) and periodic surfaces (yellow)

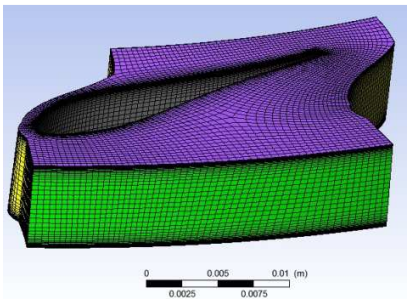

Figure 5 3D view of mesh generated for stator blade flow passage presenting inlet (green), shroud (purple) and periodic surfaces (yellow)

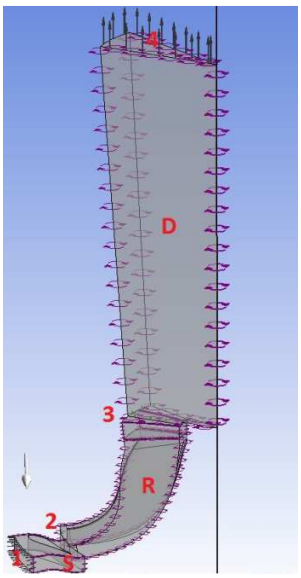

Figure 6 3D view of the computational domains and boundary conditions, including stator (S), rotor (R) and diffuser (D)

Table 1 Boundary conditions of rig (71700 RPM) and engine (106588 RPM) condition

ω (RPM)	$P_{T,s,in}$ (kPa)	$P_{S,d,out}$ (kPa)	$T_{T,s,in}$ (K)
106588	580.4	101.8	1056.5
71700	413.6	72.4	477.6

RESULTS AND DISSCUSION

Conducting CFD analysis, it was found that for both engine and rig conditions with clearance, flow variables were converged where residuals reached below 10^{-5} and the average mass flow error was 0.3%. In order to validate the performance of the corrected diffuser, pressure recovery coefficient C_P is considered to be compared to experimental results, defined as the static pressure rise through the diffuser to the dynamic pressure at the diffuser inlet:

$$C_P = \frac{P_{S,d,out} - P_{S,d,in}}{0.5\rho U_{d,in}^2} \quad (1)$$

where $P_{S,d,out}$ and $P_{S,d,in}$ are the average static pressures at the inlet and outlet of the diffuser, respectively and ρ is the fluid density and $U_{d,in}$ is the average velocity at diffuser inlet. Results show the recovery pressure coefficient expressed by equation (1) at the rig condition is 0.55 which is identical to Jones' experimental results [5, 13] reported C_P = 0.55.

3D contours of static temperature and pressure through stator and rotor flow passage are presented in Figure 7. As shown in Figure 7.a, the highest static temperature occurs at the stator inlet, decreasing throughout stator and rotor flow passages and reaches its minimum value of $T_{S,r,out}$=302 K at the rotor outlet. The static pressure distribution is shown in Figure 7.b where it reduces from $P_{S,s,in}$=413 kPa to $P_{S,r,out}$=67.323 kPa at the stator entrance and rotor exit, respectively. 3D contours of static temperature and pressure on periodic surfaces are also presented in Appendix; (Figure 12) including those through the diffuser.

Figure 8.a presents the 3D velocity magnitude distribution, illustrating the maximum velocity magnitude at the stator flow passage outlet of $U_{s,out}$ =465 *m/s*. A significant low-speed area is observed on the suction side of the rotor blades similar to what reported and discussed in [13]. Studying Mach number distribution shows that the maximum Mach number of 1.2 occurs at the stator flow passage outlet and the nozzle is chocked (shown in Figure 8.b) whereas the turbine was designed to work with a high subsonic flow [5, 13]. 3D contours of velocity magnitude and Mach number on periodic surfaces are also provided in Appendix; Figure 13 including those through the diffuser.

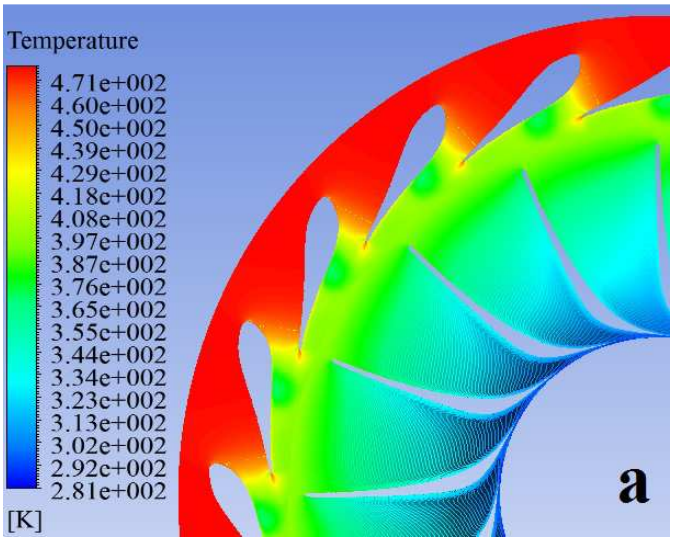

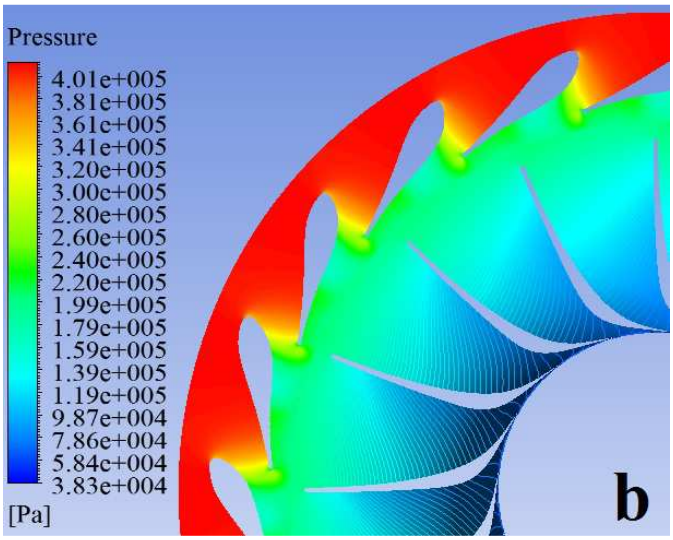

Figure 7 3D a) Static temperature and b) static pressure distribution on stator and rotor flow passages at span 0.5, rig condition

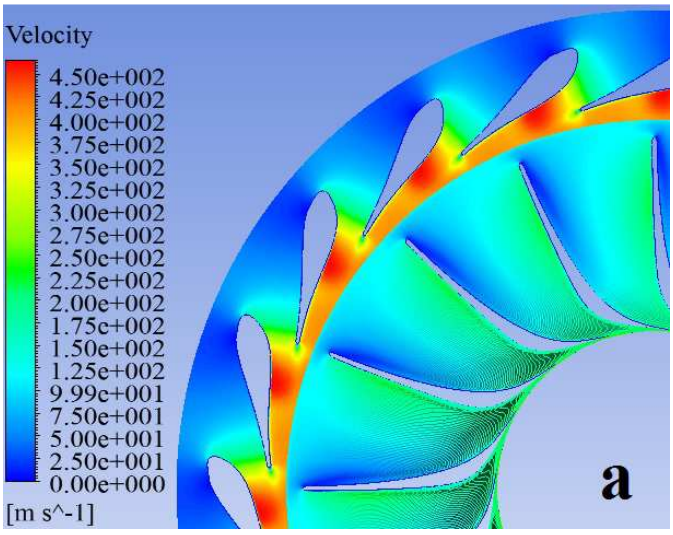

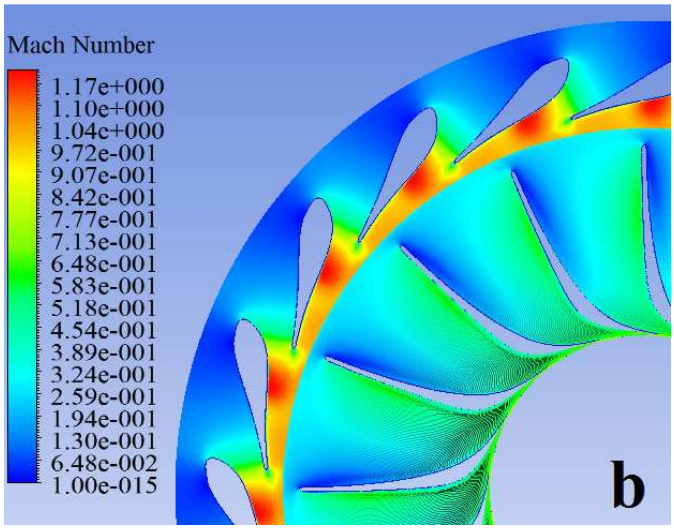

Figure 8 3D a) velocity magnitude and b) Mach number distribution on stator and rotor flow passages at span 0.5, rig condition

Total-to-static and total-to-total efficiencies are plotted in Figure 10 and 11 comparing the results of CFX to those of numerical and experimental investigations conducted in [5, 13]. Considering the total-to-static efficiency between the stator inlet and diffuser outlet at rig condition (71700 RPM), CFX reaches around 6% lower total-to-static efficiency compared to that of Pushbutton and experiment while the CFX total-to-static efficiency at engine condition (106588 RPM) demonstrates a good agreement with that of meanline design.

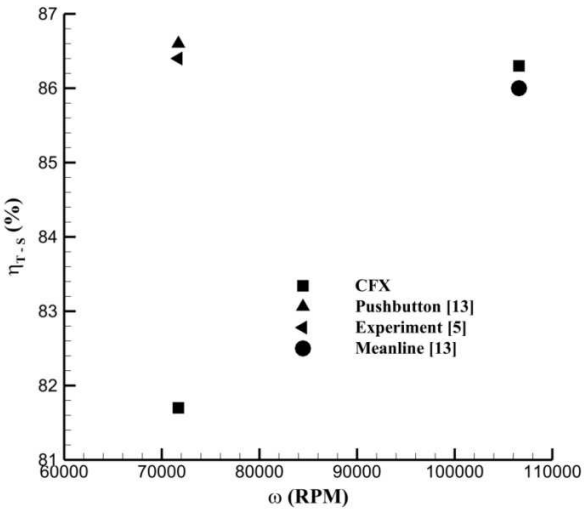

Figure 9 Total-to-static efficiency variations vs. rotation speed

Figure 11 illustrates 6% difference between the total-to-total efficiency of CFX and that of experiment where this increases to 8% while CFX total-to-total efficiency is compared to that of Pushbutton at rig condition. The results of CFX and meanline

study display an almost identical total-to-total efficiency at engine condition.

One should note that to decrease the efficiency difference conducted by CFX and Pushbutton/experiment, higher resolution advection scheme and turbulence numeric should be considered for both rig and engine conditions. It is also interesting to run the solver with other turbulent models and compare the outcomes with experimental data. This, however, is left for a future report.

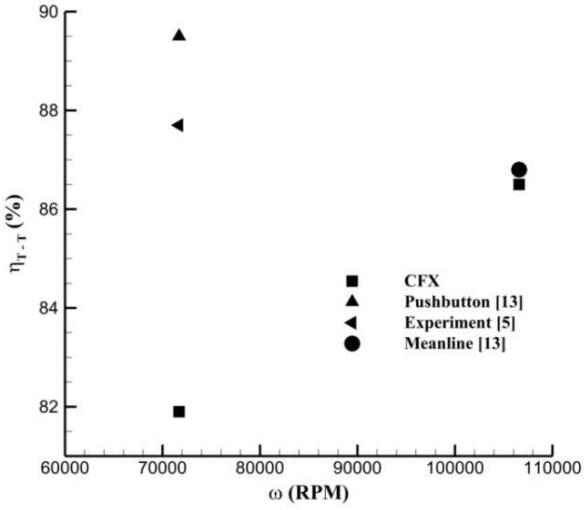

Figure 10 Total-to-total efficiency variations vs. rotation speed

CONCLUSION

The aim of the present study is to reproduce the closest geometry of a high pressure ratio single stage radial-inflow turbine applied in the Sundstrans Power Systems T-100 Multipurpose Small Power Unit. The commercial software ANSYS-Vista RTD, Blade Gen, TurboGrid and CFX are used to perform a meanline design, create 3D geometry of one flow passage and conduct three-dimensional Reynolds-Averaged Navier-Stokes (RANS) equations respectively. The proposed design of the exciting turbine is carefully examined against the fully-opened published geometrical data and results confirm that the correct 3D geometry is successfully reproduced. It was observed that the correct diffuser created by ANSYS-Geometry improved its performance compared to experimental data. The comparison between CFX and available numerical and experimental results show a good agreement and validate the CFD simulations where the maximum of 6% efficiency difference is obtained by comparing the CFX and experimental results.

ACKNOWLEDGMENT

This research was performed as part of the Australian Solar Thermal Research Initiative (ASTRI), a project supported by the Australian Government, through the Australian Renewable Energy Agency (ARENA).

REFERENCES

[1] Boyce, M.P., 8 - Radial-Inflow Turbines, in Gas Turbine Engineering Handbook (Fourth Edition), M.P. Boyce, Editor. 2012, Butterworth-Heinemann: Oxford. p. 357-383.

[2] Hiett, G. and I. Johnston. Experiments concerning the aerodynamic performance of inward flow radial turbines. in Proceedings of the Institution of Mechanical Engineers. 1936.

[3] Holeski, D.E. and M.G. Kofskey, Cold performance evaluation of a 6.02-inch radial inflow turbine designed for a 10-kilowatt shaft output Brayton cycle space power generation system, in NASA Technical Report. 1966, NASA Lewis Research Center; Cleveland, OH, United States.

[4] Stephen Spence and D. Artt, Experimental performance evaluation of a 99.0 mm radial inflow nozzled turbine with different stator throat areas. Proceedings of the Institution of Mechanical Engineers, Part A: Journal of Power and Energy, 1997. 211(A6): p. 477-488.

[5] Jones, A.C., Design and Test of a Small, High Pressure Ratio Radial Turbine. Journal of Turbomachinery, 1996. 118(2): p. 362-370.

[6] Prasad, V., Numerical simulation for flow characteristics of axial flow hydraulic turbine runner. Energy Procedia, 2012. 14(0): p. 2060-2065.

[7] Simpson, A.T., S.W.T. Spence, and J.K. Watterson, Numerical and Experimental Study of the Performance Effects of Varying Vaneless Space and Vane Solidity in Radial Turbine Stators. Journal of Turbomachinery, 2013. 135(3): p. 031001-031001.

[8] Deng, Q.H., et al., Experimental and numerical investigation on overall performance of a radial inflow turbine for 100kw microturbine. Proceedings of the Asme Turbo Expo, Vol 3. 2007, New York: Amer Soc Mechanical Engineers. 919-926.

[9] Lewis Research, C. and A.J. Glassman, Computer program for design analysis of radial-inflow turbines. 1976, Washington, D.C. : [Springfield, Va.: National Aeronautics and Space Administration ; For sale by the National Technical Information Service].

[10] Choi, H.-J., et al., CFD validation of performance improvement of a 500 kW Francis turbine. Renewable Energy, 2013. 54(0): p. 111-123.

[11] Li, Y.J., Q. Zheng, and Asme, Numerical simulation of a multistage radial inflow turbine. Proceedings of the ASME Turbo Expo 2006, Vol 6, Pts A and B. 2006, New York: Amer Soc Mechanical Engineers. 1141-1148.

[12] Carrillo, R.A.M., et al., RADIAL INFLOW TURBINE ONE AND TRI-DIMENSIONAL DESIGN ANALYSIS OF 600 kW SIMPLE CYCLE GAS TURBINE ENGINE. Proceedings of the Asme Turbo Expo 2010, Vol 5. 2010, New York: Amer Soc Mechanical Engineers. 477-486.

[13] Sauret, E., OPEN DESIGN OF HIGH PRESSURE RATIO RADIAL-INFLOW TURBINE FOR
ACADEMIC VALIDATION, in ASME 2012 International Mechanical Engineering Congress & Exposition. 2012: Houston, Texas, USA.

[14] Ventura, C.A.M., et al., Preliminary Design and Performance Estimation of Radial Inflow Turbines: An Automated Approach. Journal of Fluids Engineering, 2012. 134(3): p. 031102-031102.

[15] ANSYS 15 Help.

[16] Rocha, P.A.C., et al., k–ω SST (shear stress transport) turbulence model calibration: A case study on a small scale horizontal axis wind turbine. Energy, 2014. 65(0): p. 412-418.

[17] Louda, P., et al., Numerical simulation of turbine cascade flow with blade-fluid heat exchange. Applied Mathematics and Computation, 2013. 219(13): p. 7206-7214.

APPENDIX

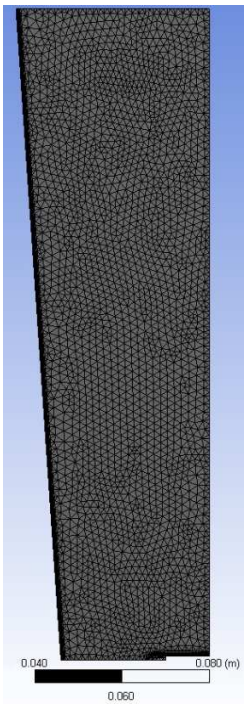

Figure 11 Diffuser mesh generated by ANSYS-Mesh

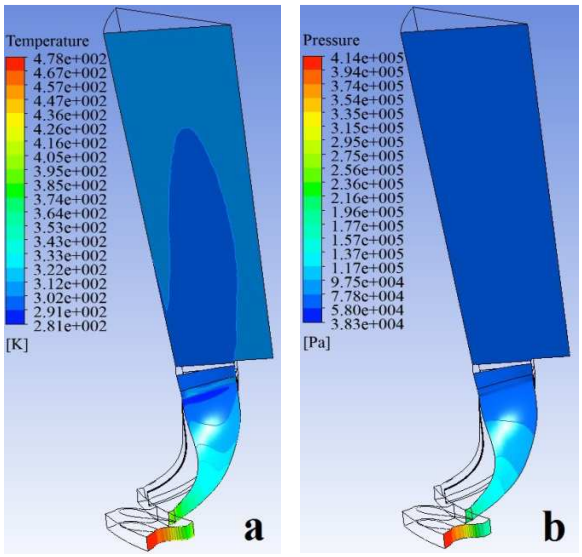

Figure 12 a) Static temperature and b) static pressure distribution on periodic surfaces of stator, rotor and diffuser

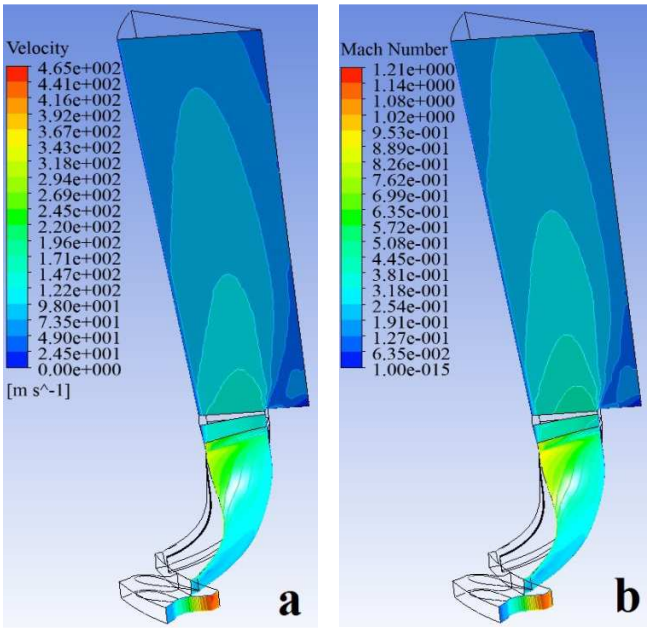

Figure 13 a) Velocity magnitude and b) Mach number distribution on periodic surfaces of stator, rotor and diffuser